J|A|C|S
ARTICLES
Published on Web 01/24/2002

Slow Internal Dynamics in Proteins: Application of NMR Relaxation Dispersion Spectroscopy to Methyl Groups in a Cavity Mutant of T4 Lysozyme

Frans A. A. Mulder,[†] Bin Hon,[‡] Anthony Mittermaier,[†] Frederick W. Dahlquist,[‡] and Lewis E. Kay*,[†]

Contribution from the Protein Engineering Network Centres of Excellence and Departments of Medical Genetics, Biochemistry and Chemistry, University of Toronto, Toronto M5S 1A8, Canada, and Institute of Molecular Biology and Department of Chemistry, University of Oregon, Eugene 97403, Oregon

Received August 15, 2001. Revised Manuscript Received October 5, 2001

Abstract: Recently developed carbon transverse relaxation dispersion experiments (Skrynnikov, N. R.; et al. *J. Am. Chem. Soc.* **2001**, *123*, 4556−4566) were applied to the study of millisecond to microsecond time scale motions in a cavity mutant of T4 lysozyme (L99A) using methyl groups as probes of dynamics. Protein expressed in *E. coli* cells with $^{13}CH_3$-pyruvate as the sole carbon source contained high levels of ^{13}C enrichment at a total of 80 Valγ, Leuδ, Ileγ_2, Alaβ, and Metϵ methyl positions with little extraneous incorporation. Data for 72 methyl groups were available for analysis. Dispersion profiles with large amplitudes were measured for many of these residues and were well fit to a two-state exchange model. The interconversion rates and populations of the states, obtained from fitting relaxation dispersion profiles of each individual probe, were remarkably homogeneous and data for nearly all methyl groups in the protein could be collectively fit to a single cooperative conformational transition. The present study demonstrates the general applicability of methyl relaxation dispersion measurements for the investigation of millisecond time scale protein motions at a large number of side-chain positions. Potential artifacts associated with the experiments are described and methods to minimize their effects presented. These experiments should be particularly well suited for probing dynamics in high molecular weight systems due to the favorable NMR spectroscopic properties of methyl groups.

Introduction

Knowledge of protein structure and dynamics is critical for a complete description of biological processes at atomic resolution.[1,2] A large number of NMR relaxation studies have reported on fast (ps−ns) protein motions;[3] however, fewer studies of slower dynamical processes (μs−ms) have appeared and consequently much less is known about motion in this regime. These slower motions are likely very important in biology. For example, enzyme catalysis and ligand off-rates in many systems are measured to be on the order of $10-10^5$/s,[4] and folding rates for small globular proteins fall in the range of $10^{-1}-10^5$/s.[5] The internal protein motions that underlie many of these phenomena will therefore have time constants in the millisecond to microsecond range. $R_{1\rho}$ and R_2 relaxation rates are very sensitive to motions on this time scale, and relaxation dispersion experiments[6−15] can be used to extract both kinetic (rate constants) and thermodynamic (populations) parameters describing dynamic processes in addition to the chemical shift differences of the interconverting sites.

We recently described in detail methods for measuring slow dynamics at side-chain positions in proteins using either AX_2 or AX_3 spin systems as motional probes.[11,12] The experiments that have been developed monitor transverse ^{15}N (NH_2) or ^{13}C (CH_3) relaxation during Carr−Purcell−Meiboom−Gill (CPMG) pulse trains,[16,17] with effective relaxation rates (on a per site basis), $R_{2,\mathrm{eff}}$, measured as a function of the average rf field strength. The dispersion profiles so generated can be fit to obtain exchange parameters.[13] Methyl groups, in particular, are ideally

[†] University of Toronto.
[‡] University of Oregon.

(1) Ishima, R.; Torchia, D. A. *Nat. Struct. Biol.* **2000**, *7*, 740−743.
(2) Kay, L. E. *Nat. Struct. Biol. NMR Suppl.* **1998**, *5*, 513−516.
(3) Palmer, A. G. *Curr. Opin. Struct. Biol.* **1997**, *7*, 732−737.
(4) Fersht, A. *Enzyme Structure and Mechanism*, 2nd ed.; Freeman & Co.: New York, 1985.
(5) Jackson, E. S. *Folding Des.* **1998**, *3*, 81−91.
(6) Allerhand, A.; Gutowsky, H. S. *J. Chem. Phys.* **1965**, *42*, 1587−1599.
(7) Davis, D. G.; Perlman, M. E.; London, R. E. *J. Magn. Reson. Ser. B* **1994**, *104*, 266−275.
(8) Akke, M.; Liu, J.; Cavanagh, J.; Erickson, H. P.; Palmer, A. G. *Nat. Struct. Biol.* **1998**, *5*, 55−59.
(9) Millet, O.; Loria, J. P.; Kroenke, C. D.; Pons, M.; Palmer, A. G. *J. Am. Chem. Soc.* **2000**, *122*, 2867−2877.
(10) Mulder, F. A. A.; van Tilborg, P. J. A.; Kaptein, R.; Boelens, R. *J. Biomol. NMR* **1999**, *13*, 275−288.
(11) Mulder, F. A. A.; Skrynnikov, N. R.; Hon, B.; Dahlquist, F. W.; Kay, L. E. *J. Am. Chem. Soc.* **2000**, *123*, 967−975.
(12) Skrynnikov, N. R.; Mulder, F. A. A.; Hon, B.; Dahlquist, F. W.; Kay, L. E. *J. Am. Chem. Soc.* **2001**, *123*, 4556−4566.
(13) Palmer, A. G.; Kroenke, C. D.; Loria, J. P. *Methods Enzymol.* **2001**, *339*, 204−238.
(14) Ishima, R.; Louis, J. M.; Torchia, D. A. *J. Am. Chem. Soc.* **1999**, *121*, 11589−11590.
(15) Ishima, R.; Torchia, D. A. *J. Biomol. NMR* **1999**, *14*, 369−72.
(16) Carr, H. Y.; Purcell, E. M. *Phys. Rev.* **1954**, *4*, 630−638.
(17) Meiboom, S.; Gill, D. *Rev. Sci. Instrum.* **1958**, *29*, 688−697.

suited for the study of protein dynamics by NMR spin relaxation methods[14,18,19]. The 3-fold rotation of the methyl scales its ^{13}C relaxation rate by 1/9, resulting in narrow spectral lines, even for proteins with moderately large molecular weights.[20]

Despite the spectroscopic sensitivity of methyl groups, experiments remain, nevertheless, only practical in cases of isotopic enrichment. In this regard, the simplest approach is to produce uniformly ^{13}C labeled samples. In practice, however, the large one-bond $^{13}C-^{13}C$ coupling and the nonvanishing longer range carbon homonuclear couplings complicate extraction of reliable relaxation rates, since during the application of the CPMG pulse trains magnetization is interchanged among spins within the coupled carbon network by homonuclear Hartmann−Hahn effects.[21] With this problem in mind, our previous studies had been limited to applications involving methionine methyls in uniformly ^{13}C labeled samples.[12] To extend the methodology to other side-chain positions, proteins must first be prepared with ^{13}C enrichment only at methyl carbon sites. In this regard, the use of $^{13}CH_3$-pyruvate ($^{13}CH_3{}^{12}CO{}^{12}COO^-$) is particularly attractive. Rosen et al.[22] and subsequently Wand and co-workers[23] showed that the ^{13}C label of pyruvate is incorporated with high yield into the methyl groups of Val, Leu, Ile(γ_2), and Ala, and with the exception of Ala, one-bond couplings between the methyl and the adjacent carbon nucleus are essentially absent. We have observed that, additionally, a high level of enrichment is also obtained for Met methyl groups. It is possible, therefore, to obtain dispersion profiles for all methyl-bearing residue types, with the exception of Thr, using this labeling procedure.

Herein we describe the application of $^{13}CH_3$ transverse relaxation dispersion NMR experiments to the study of conformational exchange in a cavity mutant form of T4 lysozyme (T4L), labeled with ^{13}C at methyl positions using $^{13}CH_3$-pyruvate. The substitution of Ala for Leu in the C-terminal domain of T4L (L99A) creates a completely buried, hydrophobic cavity of ~150 Å^3.[24] Although this cavity is inaccessible in static structures, L99A binds small hydrophobic ligands, such as substituted benzenes, in a rapid and reversible manner.[25] Clearly excursions from the inaccessible state must occur to allow for ligand entry and exit, and as we show below, relaxation dispersion NMR spectroscopy can be used to probe these events. Methyl groups are particularly powerful reporters of dynamics in the present case since the cavity is lined almost exclusively with methyl-containing residues. Dispersion profiles were obtained for a large number of side-chain methyl sites throughout the protein and were well fit to a two-site exchange model.[26] The picture that emerges is one in which L99A exists predominantly in a closed form that is impermeable to ligand with exchange ($k_{closed,open} \sim 50\ s^{-1}$, $k_{open,closed} \sim 1400\ s^{-1}$, 25 °C) to an open, ligand-receptive state that is 2.0 kcal/mol higher in free energy (3.4% fractional population at 25 °C). These results substantiate previous relaxation dispersion studies of T4 lysozyme L99A, using backbone ^{15}NH, side-chain $^{15}NH_2$ (Asn,Gln) and side-chain $^{13}CH_3$ (Met) probes.[11,12,27]

Materials and Methods

Sample Preparation. Protein was expressed and purified essentially as described previously.[28] Cysteine-free protein, WT* (C54T/C97A), and the L99A mutant (Leu99Ala in cysteine-free background WT*) were overexpressed in *Escherichia coli* (bacterial strain K38) with $^{13}CH_3$-pyruvate (4 g/L) and $^{15}NH_4Cl$ as the sole carbon and nitrogen sources, respectively. The bacteria were grown in 5 mL of LBH media at 37 °C for ~10 h and subsequently moved to 25 mL of M9T media overnight. The culture was then added to 1 L of M9T media, and the cells were allowed to grow until an OD_{600} of 0.8. At this point, the temperature was reduced to 25 °C and after 30 min 0.3 g of IPTG was added to induce protein expression. The bacteria were harvested 12 h later (OD_{600} of 1), although this time can be shorter. It is noteworthy that when glucose is substituted for pyruvate cell densities on the order of 1.15 are achieved prior to harvesting. We have found that similar levels of protein expression are obtained using either pyruvate or glucose; however, growth rates are reduced by ~50% when pyruvate is employed. NMR samples were 1.0 (L99A) or 2.0 mM (WT*) protein in 50 mM P_i, 25 mM NaCl, pH 5.5, 5% ^2H_2O. Although ^{15}N labeling is not required for the experiments described below, we prefer to produce ^{15}N-labeled samples so that the integrity of the protein can be checked in a rapid manner by recording $^1H-^{15}N$ HSQC spectra.

Methyl Relaxation Dispersion Experiments. The pulse sequence used to measure relaxation dispersion profiles of ^{13}C-methyl spins is shown in Figure 1a. The pulse sequence is very similar to that described previously,[12] with an optional purging period prepended to remove magnetization derived from the (significant) fraction of molecules where Ala is enriched at both methyl (Cβ) and Cα positions. The purging element in the experiment is illustrated between brackets. During the delay, $2\tau_C = 1/2J_{CC}$, with J_{CC} the one-bond $^{13}C-^{13}C$ coupling constant, $^{13}C\beta$ magnetization becomes antiphase with respect to the attached $^{13}C\alpha$ carbon. The subsequent ^{13}C 90° pulse converts the magnetization into zero/double quantum coherences which are dephased during the period $\zeta-180^{C\alpha}-\zeta$ by the pulsed field gradient pair of magnitude g3. All methyl groups without directly attached ^{13}C spins are essentially unaffected by this filtration step since the carbon pulse at the end of the $2\tau_C$ period restores uncoupled magnetization to the *Z*-axis. However, all methyls experience a sensitivity loss due to transverse relaxation decay (~40% in L99A) during the $2\tau_C$ (~14 ms) element. If sensitivity is limiting, therefore, it may be advantageous to record dispersion profiles for all non-Ala residues without this purging element, as we have done in the present application. With regard to sensitivity, we note in passing that the sequence of Figure 1 (without the purging element) has been applied successfully to lysozyme samples at 10 °C, where the overall tumbling time is on the order of 20 ns.[29] As a final note, a ^1H 90° pulse is applied after the $2\tau_C$ delay to purge coherences created by $^1H-^{13}C$ dipole−dipole cross-correlated spin relaxation during this period. In this way, magnetization immediately preceding the CPMG period (point a in the figure) is in-phase along the *Y*-axis.

Experiments were recorded on Varian Inova spectrometers, operating at 600- and 800-MHz ^1H frequencies and at a probe temperature of 25 °C. The experiments and data analysis were performed as described previously.[12] Briefly, CPMG pulse trains attenuate chemical exchange

(18) Muhandiram, D. R.; Yamazaki, T.; Sykes, B. D.; Kay, L. E. *J. Am. Chem. Soc.* **1995**, *117*, 11536−11544.
(19) Henry, G. D.; Weiner, J. H.; Sykes, B. D. *Biochemistry* **1986**, *25*, 590−598.
(20) Kay, L. E.; Bull, T. E.; Nicholson, L. K.; Griesinger, C.; Schwalbe, H.; Bax, A.; Torchia, D. A. *J. Magn. Reson.* **1992**, *100*, 538−558.
(21) Ernst, R. R.; Bodenhausen, G.; Wokaun, A. *Principles of Nuclear Magnetic Resonance in One and Two Dimensions*; Oxford University Press: Oxford, U.K., 1987.
(22) Rosen, M. K.; Gardner, K. H.; Willis, R. C.; Parris, W. E.; Pawson, T.; Kay, L. E. *J. Mol. Biol.* **1996**, *263*, 627−636.
(23) Lee, A. L.; Urbauer, J. L.; Wand, A. J. *J. Biomol. NMR* **1997**, *9*, 437−440.
(24) Eriksson, A. E.; Baase, W. A.; Zhang, X. J.; Heinz, D. W.; Blaber, M.; Baldwin, E. P.; Matthews, B. W. *Science* **1992**, *255*, 178−183.
(25) Feher, V. A.; Baldwin, E. P.; Dahlquist, F. W. *Nat. Struct. Biol.* **1996**, *3*, 516−521.
(26) Carver, J. P.; Richards, R. E. *J. Magn. Reson.* **1972**, *6*, 89−105.
(27) Mulder, F. A. A.; Hon, B.; Muhandiram, D. R.; Dahlquist, F. W.; Kay, L. E. *Biochemistry* **2000**, *39*, 12614−12622.
(28) Matsumura, M.; Becktel, W. J.; Matthews, B. W. *Nature* **1988**, *334*, 406−410.
(29) Mulder, F. A. A.; Mittermaier, A.; Hon, B.; Dahlquist, F. W.; Kay, L. E. *Nat. Struct. Biol.* **2001**, *8*, 932−935.

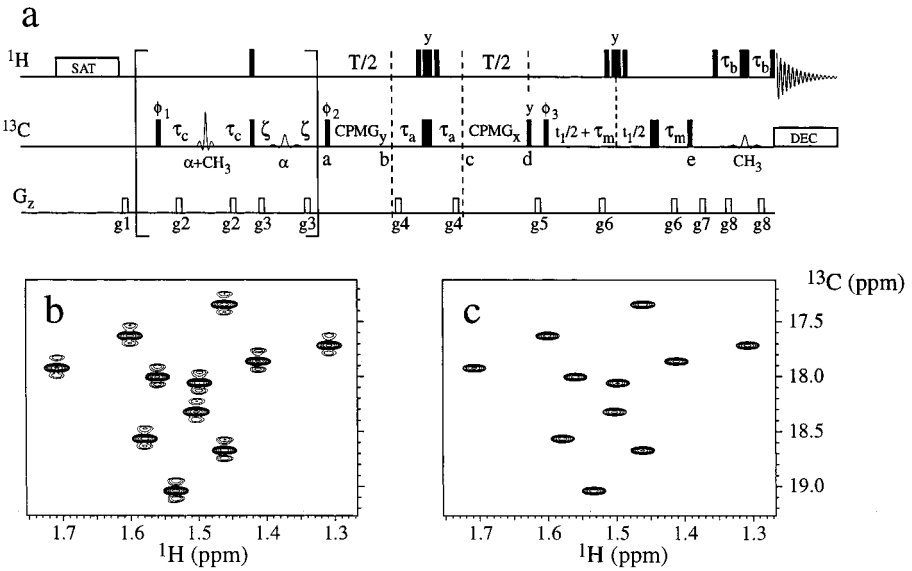

Figure 1. (a) Pulse scheme used to measure transverse ^{13}C relaxation dispersion profiles of CH_3 groups in proteins labeled at Ala, Leu, Val, Ile (γ_2), and Met methyl-positions. All narrow (wide) rectangular pulses are applied with flip angles of 90° (180°) along the *x*-axis, unless indicated otherwise. ^{1}H pulses used for the NOE buildup at the start of the sequence are applied with 120° flip angles[42] at spacings of 5 ms using a 7.5-kHz field. All other ^{1}H pulses use a field of 37 kHz. The ^{1}H carrier is centered at 1.0 ppm until immediately after the final ^{13}C 90° pulse (point e) when it is jumped to 4.7 ppm (water). All rectangular ^{13}C pulses (centered at 21 ppm) employ a field of 12.5 kHz between points a and d, with all remaining rectangular pulses applied with an 18.8-kHz field. The shaped ^{13}C pulses have a REBURP profile[35] with the first REBURP pulse, 400 μs (600 MHz), centered at 36 ppm exciting the complete aliphatic region. The second REBURP pulse, 1.6 ms (600 MHz), is centered at 53 ppm through phase modulation of the rf[43,44] to selectively refocus Cα magnetization of the Ala spins. The final REBURP pulse, 1.6 ms at 600 MHz, is applied on-resonance (21 ppm) to eliminate all ^{1}H−^{13}C correlations that are downfield of 30 ppm in the carbon dimension. ^{13}C Decoupling during acquisition is achieved using a 2.5-kHz WALTZ-16 scheme.[45] Each CPMG$_y$ train is of the form $(\tau-180^\circ_y-\tau)_{n/2}$, with $T = n(2\tau + pw_C^{180^\circ})$, with $pw_C^{180^\circ}$ the ^{13}C 180° pulse width, and $n/2$ is even. The 180° pulses during the CPMG periods have the REBURP shape (500 μs, 12.2 kHz peak rf field). These pulses are centered at 8 (600 MHz) or 20.2 ppm (800 MHz) so that the a null is obtained at the resonance positions of the Leu Cα carbons. The delays used are as follows: $T = 40$ ms, $\tau_a = 1/4J_{CH} = 2.0$ ms, $\tau_m = 0.7838$ ms ($2\pi J_{CH}\tau_m = 0.6158$), $\tau_b = 2.0$ ms, $\tau_c = 1/4J_{CC} = 7.33$ ms, and $\zeta = 1.0$ ms. Note that $2\tau_c$ ($2\tau_b$) refers to the delays between successive ^{13}C (^{1}H) 90° pulses. The phase cycle is as follows: $\phi1 = (x,-x)$; $\phi2 = 2(x),2(-x)$; $\phi3 = 4(x),4(-x)$; rec = $x,2(-x),x,-x,2(x),-x$. Quadrature detection in F_1 is achieved using States-TPPI[46] of $\phi3$. The strengths and durations of the gradients are as follows: g1 = (1 ms, 5 G/cm); g2 = (0.8 ms, 8 G/cm); g3 = (0.7 ms, 18 G/cm); g4 = (0.6 ms, 20 G/cm); g5 = (0.5 ms, −15 G/cm); g6 = (0.1 ms, 10 G/cm); g7 = (0.6 ms, 12 G/cm); g8 = (0.3 ms, 12 G/cm). Note that the portion of the sequence in brackets is used to purge signals from Ala residues that are labeled at both Cα and Cβ positions with ^{13}C. In cases where sensitivity is limiting, this scheme should be turned off when data for the other methyl groups are recorded and the phase cycling becomes $\phi2 = x,-x$; $\phi3 = 2(x),2(-x)$; rec = $x,2(-x),x$. (b) Portion of the 2D ^{1}H−^{13}C correlation spectrum containing Ala residues, obtained with a long acquisition time in the indirect ^{13}C dimension (110 ms), *without* (b) and *with* (c) the purge element shown in brackets. The spectra in panels b and c were obtained under identical experimental conditions and are drawn with the same contour levels.

dephasing as a function of the variable spin−echo pulse spacing during the constant relaxation time $T = 40$ ms. Peak intensities, $I(\nu_{CPMG})$, were obtained from a series of 20 2D correlation maps, measured with values of the average CPMG field strength, $\nu_{CPMG} = {}^1/_{4\tau_{CPMG}}$ (Hz), of 50 (2×), 100, 150 (2×), 200, 250 (2×), 300, 350 (2×), 400, 500 (2×), 600, 700, 800, 900, and 1000 (2×), where $2\tau_{CPMG}$ is the time between the centers of successive 180° pulses. In addition, reference intensities $I(0)$ were obtained from a spectrum recorded with the periods a−b and c−d in Figure 1a removed. The total measurement time required to obtain a dispersion profile at one spectrometer field was ∼21 h (1 h/2D spectrum). Uncertainties in the relative intensities of cross-peaks, σ_I, were estimated from the rmsd of duplicates (6 pairs) at each spectrometer field according to the relation, $\sigma_I = (\sum(\Delta I/I_{av})^2/2N)^{1/2}$, where the summation extends over all $N = 6$ duplicates, ΔI is the difference in peak intensities from repeat measurements and I_{av} is the average intensity of a cross-peak that is obtained in experiments that are repeated. Plots of $R_{2,eff} = (-\ln\{I(\nu_{CPMG})/I(0)\})/T$ versus ν_{CPMG} form relaxation dispersion profiles that can be fit to analytical expressions for chemical exchange[13,26,30] to obtain the parameters that characterize the microscopic exchange process.

The data obtained at two B_0 fields were fitted to three progressively more complex functions describing the dispersion profile, and *F*-statistics[31] were used to assess whether a description of the exchange process involving each of the more complicated models was warranted at the 99.9% confidence level. The first model assumes that there is no exchange, and the experimental data points are fitted to flat lines with $R_{2,eff}(\nu_{CPMG} \rightarrow \infty)$ at each B_0 field as adjustable parameters. In the second model, it is assumed that a fast-exchange process is responsible for the dispersion profile[32] and an additional pair of parameters, $\Phi_{ex} = p_A p_B \delta\omega^2$ and $\tau_{ex} = {}^1/_{(k_{AB} + k_{BA})}$ are included in the fit. Here k_{AB} and k_{BA} are the forward ($A \rightarrow B$) and backward ($B \rightarrow A$) interconversion rates, p_A and p_B are the populations of the two states, and $\delta\omega$ is the chemical shift difference between them. Finally, the third model uses the two-site exchange equation valid for all time scales of exchange;[26,30] in the case where the exchange is not fast, it is often possible to separate the product $p_A p_B \delta\omega^2$ into the individual parameters, $p_A = 1 - p_B$ and $\delta\omega$. Thus, the fitting parameters in this case are $R_{2,eff}(\nu_{CPMG} \rightarrow \infty)$ at each B_0 field, p_A, $\delta\omega$, and τ_{ex}. Note that in all of the analyses we have assumed that the intrinsic relaxation rates of the methyl carbons in each site are the same. The general two-site equation was originally derived by Carver and Richards[26] and later Jen[30] (referred to in what follows as the CRJ equation) and is approximate, since only one of the two exponential decay terms necessary to completely describe the dispersion profile is included in the analytical expression.[6] The CRJ equation is suitable for the analysis of intermediate ($\delta\omega \approx k_{ex} = k_{AB} + k_{BA}$) to fast ($\delta\omega < k_{ex}$) exchange processes but not for events that are in slow exchange ($\delta\omega > k_{ex}$). To ascertain that accurate exchange parameters could be extracted from fits of the data to the CRJ equation, the data

(30) Jen, J. *J. Magn. Reson.* **1978**, *30*, 111−128.
(31) Mosteller, F.; Tukey, J. W. *Data Analysis and Regression: A Second Course in Statistics.*; Addison-Wesley: Reading, MA, 1977.
(32) Luz, Z.; Meiboom, S. *J. Chem. Phys.* **1963**, *39*, 366−370.

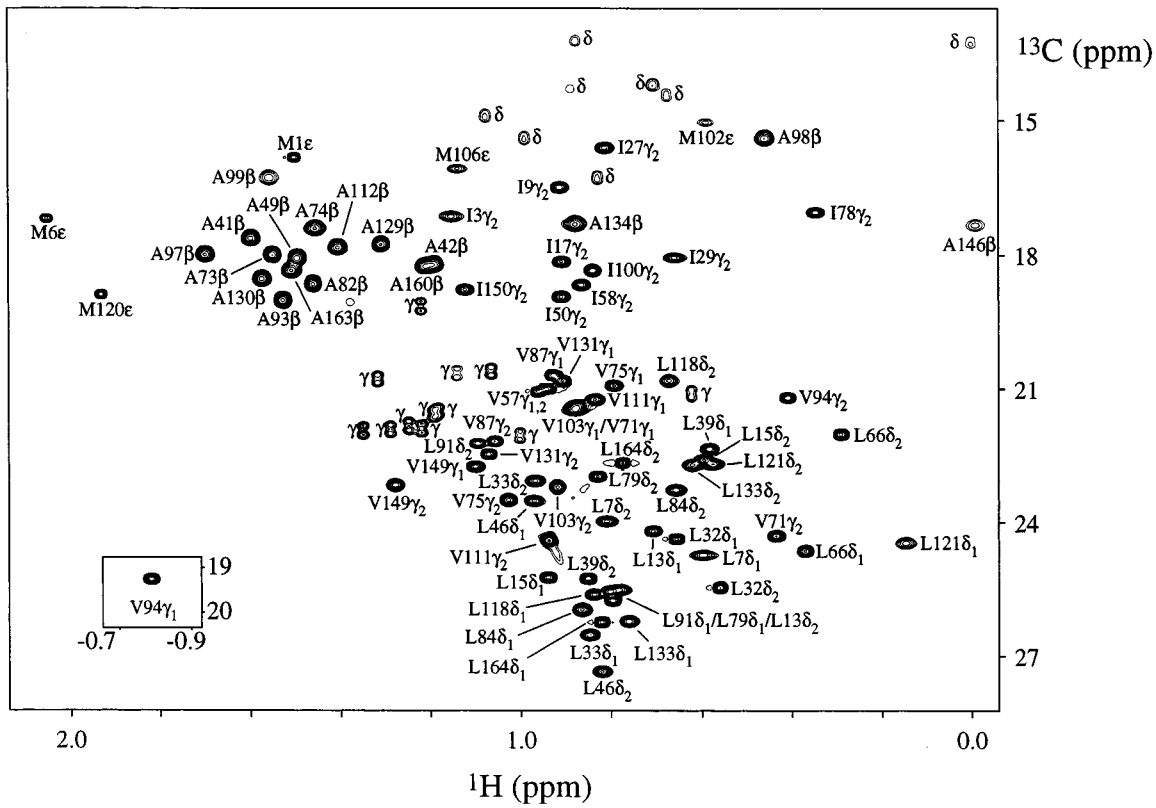

Figure 2. Reference 2D $^{1}H-^{13}C$ data set obtained *without* the purge element in the pulse scheme of Figure 1a. Assignments for all Alaβ, Valγ, Leuδ, Ileγ_2, and Metϵ methyls are given. Ileδ_1 are indicated with "δ" and Thrγ_2 are labeled "γ". All Val and Leu methyl groups have been stereospecifically assigned using the method of Neri et al.[47]

were also fitted to the complete analytical solution of two-site chemical exchange that retains both exponential functions.[6] The parameters extracted from fits to the CRJ solution were within 1−2% of those obtained using the more complex set of equations (40 lines!). The good agreement obtained with the two equations results from the fact that the exchange processes in L99A are intermediate to fast on the NMR chemical shift time scale.

Long-Range $^{13}C-^{13}C$ Coupling Experiment. A 3D long-range $^{13}C-^{13}C$ *J*-coupling experiment[33] was carried out on the WT* sample in order to ascertain how much extraneous labeling in methyl-containing side chains occurs using the pyruvate labeling strategy discussed above. The details of the experiment are as described in the original reference.[33] Diagonal and cross-peak intensities (I_{diag} and I_{cross}) were obtained from $^{1}H-^{13}C$ planes and fitted to the relation, $J_{CC} = (-1 / 2\pi T_C)$ Arctan $\sqrt{I_{cross} / I_{diag}}$ where J_{CC} is the $^{13}C-^{13}C$ scalar coupling constant, and 2Tc is the buildup time of the cross-peak (58.0 ms). Data were acquired on a Varian Inova spectrometer, operating at 500 MHz ^{1}H frequency and at a probe temperature of 25 °C.

Simulations of Chemical Exchange during CPMG Experiments. Simulations of the homogeneous McConnell equations were carried out to evaluate the effect of finite pulse widths on exchange parameters extracted from spin−echo dispersion profiles since the equations that fit the dispersion profiles neglect evolution during the pulses. Following the procedure of Helgstrand et al.,[34] an effective propagator was constructed to describe the evolution of magnetization during the constant relaxation time CPMG experiment shown in Figure 1. Constant-time relaxation dispersion profiles were simulated by assuming values that are typical in our experiments: $T = 40$ ms, rectangular pulse rf field strength of 12.5 kHz (corresponding to a 40 μs ^{13}C 180° pulse), and REBURP pulses[35] applied with a peak rf field strength of 12.3 kHz (corresponding to a 500 μs ^{13}C 180° pulse). Exchange parameters were chosen that reflect the exchange process in T4 lysozyme L99A at 25 °C: $k_{AB} = 49$ s^{-1}, $k_{BA} = 1400$ s^{-1} with effective transverse and longitudinal rates (assumed the same for both sites) of 14 and 1 s^{-1}, respectively. The number of even echoes ($\tau_{CPMG}-180°-\tau_{CPMG})_{2m}$, was varied ($1 \le m \le 40$), and dispersions were calculated for the range of chemical shift differences extracted from the experimental data. Profiles were obtained using either rectangular (40 μs) or REBURP pulses (500 μs, see below) and compared to evaluate the effects of exchange during the longer REBURP pulses.

Results and Discussion

Protein Samples from $^{13}CH_3$-Pyruvate as the Carbon Precursor. Protein samples prepared using $^{13}CH_3$-pyruvate as the sole carbon source showed high levels of enrichment of ^{13}C label at methyl positions and generally low levels of enrichment at non-methyl sites. Figure 2 illustrates a 2D $^{13}C-^{1}H$ correlation spectrum for L99A, obtained with the pulse sequence of Figure 1a. Val, Leu, and Ile (γ2) methyl groups give rise to strong correlations with no doublet components of intensity larger than 3% (sum of outer lines relative to inner singlet) due to the presence of a ^{13}C isotope at the adjacent carbon position. In contrast, Ala residues were found to have rather high (20−45%, depending on the sample) levels of enrichment at $^{13}C\alpha$, which gives rise to an unresolved superposition of singlets ($^{13}C\beta-^{12}C\alpha$) and doublets ($^{13}C\beta$-$^{13}C\alpha$), as can be seen in Figure 2. Shown in panels b and c of Figure 1 are portions of spectra recorded with very high resolution in the indirect dimension, *without* (b) and *with* (c) the purging period in the pulse scheme (Figure 1a; see Materials and Methods). Extraction of accurate $R_{2,eff}$ values from analysis of the central Ala line is, in general,

(33) Bax, A.; Max, D.; Zax, D. *J. Am. Chem. Soc.* **1992**, *114*, 6923−6925.
(34) Helgstrand, M.; Hard, T.; Allard, P. *J. Biomol. NMR* **2000**, *18*, 49−63.
(35) Geen, H.; Freeman, R. *J. Magn. Reson.* **1991**, *93*, 93−141.

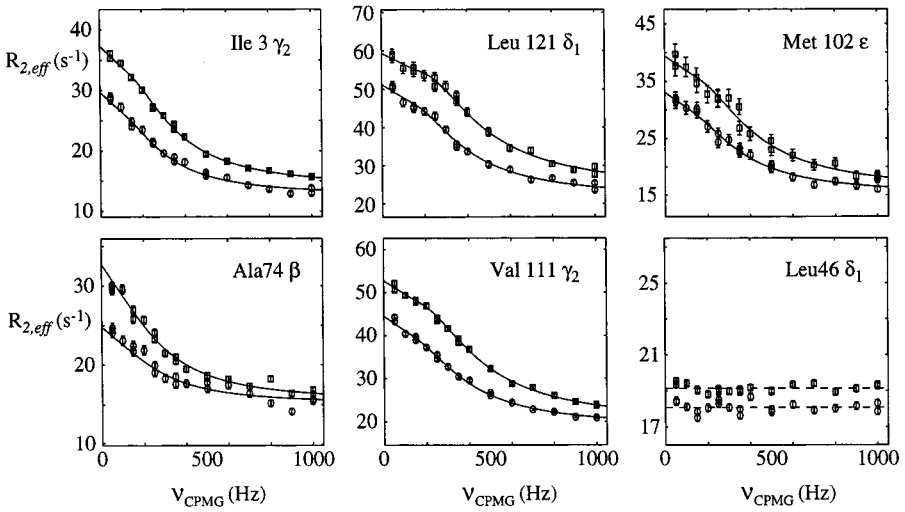

Figure 3. Representative methyl transverse ^{13}C relaxation dispersion profiles recorded at 600 (circles) and 800 MHz (squares) for T4 lysozyme L99A. Leu46δ_1 is shown as an example of a residue without conformational exchange. The parameters obtained from fitting the profiles along with fitting statistics are given in Table 1.

difficult and we prefer to obtain relaxation dispersion data for Ala from spectra where the doublets are purged (c). We have also observed small levels of enrichment at Ile (δ1) and Thr (γ2) methyl positions (Figure 2) due to scrambling of the isotope label and like the case of Ala, these signals are composed of both singlet and doublet components. Also noted is the high incorporation (>80%) of ^{13}C at Met methyl groups. Interestingly, the ϵCH_3 group of Met derives from the Ser Cβ group, the precursor of which is the ^{13}C-methyl of pyruvate.[36,37] Strangely, however, standard $^1H-^{13}C$ HSQC spectra did not show high levels of $^{13}C\beta$ labeling in Ser residues of lysozyme samples prepared with ^{13}C-methyl pyruvate.

Methyl Relaxation Dispersion Measurements. T4 lysozyme L99A is comprised of 164 amino acids with 102 methyl groups. Using $^{13}CH_3$-pyruvate as precursor, 80 of the methyl groups were labeled to a high extent and 72 nonoverlapping cross-peaks that were amenable to analysis were observed in 2D $^{13}C-^1H$ correlation maps. Representative methyl carbon relaxation data are shown in Figure 3 for the different amino acid types that are available using the pyruvate labeling protocol. In total, 15 residues gave flat dispersion profiles, indicating the absence of an exchange contribution to the methyl carbon line width, 47 residues were fit appropriately by the fast-exchange equation, and 8 residues were fit by the CRJ equation. The dispersions for Ala99 and -146 were not fitted on an individual basis since the correlations for these residues were extremely weak. The extracted parameters are given in Table 1. In the majority of cases, the data was well fit. For example, an average reduced χ^2 value, χ_ν^2, of 1.7 $\pm$ 1.1 was obtained from fits of dispersion profiles for the 55 residues that were best modeled with either the fast-exchange[32] or CRJ equations.[26,30] In some cases, larger χ_ν^2 values were obtained when the amplitude of the dispersion profile was very small; in these cases, the profiles were best fit to straight lines. Of interest, methyl dispersion profiles for T4 lysozyme WT* show no evidence of the exchange process that is present in the L99A mutant (i.e., all profiles are flat).

Practical Aspects of Methyl Relaxation Dispersion Measurements. There are a number of potential systematic errors associated with CPMG experiments, and we consider here the two major ones. First, the finite width of each of the refocusing pulses during the CPMG interval(s) causes magnetization to be effectively tilted out of the transverse plane during application of the pulses. An accurate description of the evolution of magnetization thus requires that the trajectory and the relaxation of magnetization during the trajectory be evaluated.[38,39] These effects are expected to be of relatively minor importance for methyl carbon nuclei, as compared with ^{15}N, since for the same power deposition in the sample during the CPMG intervals of Figure 1 the ^{13}C pulse width is a factor of $|\gamma_C/\gamma_N|^2$ smaller. Nonetheless, simulations establish that slightly reduced relaxation rates (by $\sim$0.5 s^{-1}) may be obtained at the highest of pulse repetition rates for resonances that are near the border of the ^{13}C spectrum using 40 μs rectangular or 500 μs REBURP (see below) 180° refocusing pulses.

The second source of error is due to the fact that during CPMG experiments homonuclear scalar couplings will cause the magnetization of interest to exchange with magnetization from other nuclei in the side chain. This Hartmann−Hahn mixing will depend in an intricate way on the CPMG pulse rate, on the number of nuclei in the coupling network and their frequency offsets, and, in the current case, on the level of ^{13}C isotope enrichment throughout the side chain. As discussed previously, with the exception of Ala, one-bond $^{13}C-^{13}C$ couplings involving methyl groups are essentially nonexistent for samples derived from $^{13}CH_3$-pyruvate. However, some "metabolic conversion" of the ^{13}C-methyl label does occur and ^{13}C incorporation has been observed at non-methyl sites. To establish whether the long-range couplings to the methyls that derive from this metabolic conversion interfere with the extraction of accurate exchange parameters, we have recorded methyl dispersion profiles for T4 lysozyme WT* (see Materials and Methods). As expected, most dispersion profiles were flat (since the exchange process that is present in L99A is absent

(36) Bender, D. A. *Amino Acid Metabolism*; Wiley-Interscience: New York, 1985.
(37) Gottschalk, G. *Bacterial Metabolism*; Springer-Verlag: Berlin, 1986.
(38) Ross, A.; Czisch, M.; King, G. C. *J. Magn. Reson.* **1997**, *124*, 355−365.
(39) Korzhnev, D. M.; Tischenko, E. V.; Arseniev, A. S. *J. Biomol. NMR* **2000**, *17*, 231−7.

Table 1. Exchange Parameters for Methyl Groups in T4 Lysozyme L99A[a]

methyl group	$\delta\omega$[b] (ppm)	τ_{ex} (ms)	p_B[c] (%)	$R_{2,eff}(\nu_{CPMG} \rightarrow \infty)$[d] ($s^{-1}$)		R_{ex}[d] (s^{-1})		α[e]	model[f]	χ^{2g}_{ν}	$\delta\omega_{group}$[h] (ppm)
Met1ϵ	0.48	0.22		8.3	8.5	1.5	2.7		2	3.7	-
Ile3γ_2	1.18	0.84	3.1	13.2	14.1	17.4	22.8	0.9	3	1.0	1.11
Met6ϵ	0.50	0.23		13.7	13.7	1.7	3.1		2	1.3	0.26
Leu7δ_1	0.31	1.02		15.0	15.2	2.9	5.1		2	1.4	0.36
Leu7δ_2	0.20	1.79		15.4	15.7	2.1	3.7		2	1.6	0.26
Ile9γ_2	0.39	0.44		14.4	15.0	1.9	3.4		2	1.2	0.32
Leu13δ_1	0.14	1.19		13.1	13.8	0.7	1.2		2	2.0	0.17
Leu13δ_2	0.28	1.03		13.3	13.5	2.4	4.2		2	2.0	0.33
Leu15δ_1					14.2	15.3			1	2.2	0.00
Leu15δ_2	0.11	1.57		13.7	14.6	0.6	1.0		2	1.3	0.15
Ile17γ_2[i]											0.22
Ile27γ_2	0.43	0.28		16.7	16.9	1.6	2.8		2	1.5	0.26
Ile29γ_2	0.41	0.19		13.3	14.6	0.9	1.7		2	1.2	0.18
Leu32δ_1				10.3	11.3				1	3.7	0.13
Leu32δ_2	0.57	0.72		9.5	10.9	6.9	12.3		2	1.6	0.62
Leu33δ_1	0.15	1.42		22.4	22.7	0.9	1.6		2	2.3	0.19
Leu33δ_2	0.21	1.09		19.5	20.1	1.4	2.4		2	1.8	0.25
Leu39δ_1	0.26	0.69		17.6	17.8	1.4	2.5		2	1.2	0.27
Leu39δ_2				12.4	13.5				1	2.1	0.00
Ala41β[i]									-		.20
Leu46δ_1				18.4	19.3				1	2.2	0.00
Leu46δ_2	0.16	1.05		20.6	22.2	0.8	1.5		2	1.6	0.19
Ala49β	0.28	0.75		13.1	14.6	1.8	3.1		2	1.0	0.30
Ile50γ_2[i]									-		0.24
Ile58γ_2	0.23	0.52		16.0	17.2	0.8	1.4		2	0.7	0.20
Ala63β	0.26	0.67		16.0	17.3	1.4	2.5		2	1.0	0.27
Leu66δ_1	0.42	0.90		13.2	14.2	4.6	8.2		2	1.8	-
Leu66δ_2	0.47	0.74		12.1	13.1	4.7	8.4		2	1.3	0.50
Val71γ_2	0.34	1.03		15.6	16.6	3.5	6.3		2	1.7	0.40
Ala73β	0.25	0.53		11.1	13.2	1.0	1.7		2	1.3	0.23
Ala74β	0.76	0.57		14.2	15.5	9.6	17.1		2	2.0	0.80
Val75γ_1[i]									-		-
Val75γ_2	0.66	0.64		14.9	15.9	8.1	14.4		2	2.0	0.70
Ile78γ_2	0.37	0.60		14.0	16.0	2.4	4.3		2	0.8	0.36
Leu79δ_2	0.12	1.57		13.5	14.4	0.7	1.2		2	1.2	0.16
Ala82β				10.5	12.6				1	5.0	0.12
Leu84δ_1	0.88	0.55		19.5	20.6	12.5	22.3		2	1.0	0.95
Leu84δ_2	0.34	0.79		19.4	22.3	2.7	4.9		2	1.0	0.37
Val87γ_1	0.68	0.46		16.2	18.5	6.2	11.1		2	0.8	0.61
Val87γ_2	0.55	0.45		12.0	13.7	3.9	7.0		2	0.8	0.46
Leu91δ_2				15.0	16.5				1	1.6	0.09
Ala93β				12.3	14.1				1	2.5	0.00
Val94γ_1	0.37	0.62		12.6	13.9	2.5	4.5		2	1.3	0.37
Val94γ_2	0.23	0.73		12.2	13.1	1.1	2.0		2	3.8	0.24
Ala97β	0.25	0.65		17.2	18.2	1.2	2.2		2	2.0	0.25
Ala98β	0.56	0.27		16.2	17.8	2.5	4.5		2	1.9	0.34
Ala99β[j]									-		1.64
Ile100γ_2	0.84	0.66	3.5	14.0	15.2	11.3	17.5	1.5	3	1.2	0.85
Met102ϵ	1.51	0.99	3.1	14.7	16.0	21.6	25.2	0.5	3	1.4	1.35
Val103γ_2	3.52	0.54	2.9	18.5	20.5	42.2	47.0	0.4	3	1.4	3.51
Met106ϵ	0.62	0.56		11.4	12.9	6.3	11.2		2	1.7	0.62
Val111γ_1	0.52	0.32		17.9	18.3	2.6	4.6		2	0.8	0.35
Val111γ_2	1.64	0.66	3.2	18.9	20.0	25.7	32.8	0.9	3	1.2	1.63
Ala112β				12.5	14.5				1	3.0	0.13
Leu118δ_1	0.32	0.84		17.6	18.9	2.6	4.6		2	0.8	0.36
Leu118δ_2	2.66	0.69	3.4	21.2	21.2	38.0	42.5	0.4	3	1.0	2.66
Met120ϵ	0.45	0.59		7.5	8.4	3.5	6.2		2	1.6	0.44
Leu121δ_1	1.84	0.72	3.5	19.8	22.5	30.2	36.4	0.6	3	1.2	1.88
Leu121δ_2	0.35	0.47		21.3	21.6	1.7	3.0		2	1.7	0.30
Ala129β	0.45	0.45		13.2	15.3	2.7	4.9		2	1.2	0.39
Ala130β	0.29	0.42		14.5	16.3	1.0	1.9		2	1.1	0.23
Val131γ_1				12.1	12.7				1	2.2	0.00
Val131γ_2				10.5	11.6				1	2.7	0.00
Leu133δ_1	0.64	0.59		18.9	19.9	7.1	12.6		2	1.5	0.66
Leu133δ_2	1.28	0.73	3.3	17.7	19.5	20.3	27.0	1.0	3	0.7	1.26
Ala134β	0.38	0.22		9.0	10.5	1.0	1.7		2	0.7	0.19
Ala146β[j]									-		1.48
Val149γ_1	0.28	0.69		15.3	16.7	1.6	2.9		2	0.9	0.29
Val149γ_2	0.83	0.52		16.7	17.6	10.5	18.8		2	1.0	0.85
Ile150γ_2	0.49	0.34		14.1	15.8	2.4	4.2		2	1.0	0.34

Table 1 (Continued)

methyl group	$\delta\omega^b$ (ppm)	τ_{ex} (ms)	$p_B{}^c$ (%)	$R_{2,eff}(\nu_{CPMG} \rightarrow \infty)^d$ (s^{-1})		$R_{ex}{}^d$ (s^{-1})		α^e	model^f	χ_ν^{2g}	$\delta\omega_{group}{}^h$ (ppm)
Leu164δ_1				10.8	11.2				1	8.1	-
Leu164δ_2	0.11	1.10		7.1	7.6	0.4	0.6		2	2.0	0.13

[a] Parameters obtained by fitting dispersions measured at 600 and 800 MHz simultaneously (using REBURP refocusing pulses) on a per-residue basis. [b] In cases where the fast-exchange model was applicable, $\delta\omega$ was calculated by assuming $p_A = 96.6\%$ and $p_B = 3.4\%$, as obtained from fitting all dispersion profiles together. For alternative values of the populations p_C and p_D, the shift difference can be recalculated according to $\delta\omega_{CD} = \delta\omega_{AB}\sqrt{(p_A p_B/p_C p_D)}$. [c] Population of the minor state. [d] First column $\omega_0/2\pi = 600$ MHz and, second column $\omega_0/2\pi = 800$ MHz ^{1}H Larmor frequency. $R_{ex} = R_{2,eff}(\nu_{CPMG} \rightarrow 0) - R_{2,eff}(\nu_{CPMG} \rightarrow \infty)$. [e] $\alpha = d\ \ln R_{ex}/d\ \ln\delta\omega$ defines the chemical shift time scale in the case of skewed populations: $0 \le \alpha < 1$ slow exchange; $\alpha \approx 1$ intermediate exchange; $1 < \alpha \le 2$ fast exchange.[9] Values of α are calculated from eq 20 of Millet et al.[9] and are only given if model 3 (see Materials and Methods) is required to fit the experimental data. Models: (1) no exchange; (2) fast exchange;[32] (3) exchange process best modeled with the CRJ equation.[26,30] (Data from each residue fitted independently). [g] Reduced χ^2 values obtained from fits of dispersion data on a per-residue basis. $\chi_\nu{}^2 = \chi^2/(N - m)$, where N is the number of experimental points and m is the number of parameters. The value of m is 2, 4, and 5 for models 1−3 and $N = 40$ (see Materials and Methods). $\chi^2 = \sum(R_{2,eff}^{calc} - R_{2,eff}^{expt})^2/\sigma_{R_2}{}^2$, where σ_{R_2} are the errors in $R_{2,eff}$, calculated from the fractional error in peak intensities σ_I, defined in Materials and Methods. [h] Chemical shift difference obtained from fitting each dispersion curve using values of $\tau_{ex} = 0.69$ ms and $p_B = 3.4\%$ obtained from the global fitting of all dispersion data. Residues that could not be fitted with the group parameters are indicated with a dash. [i] Good fits could not be obtained for these small-amplitude dispersions on a per-residue basis. [j] The spectral peak was too weak to accurately quantify the exchange parameters from an individual 5-parameter fit to the data. The data reported is derived from the restrained 3-parameter group fit where τ_{ex} and p_B are global parameters.

in the WT protein) and could be fitted with low residuals, but for several Leu methyl groups, apparent exchange profiles were obtained. These "false positives" had small amplitudes of 2−4 s^{-1}, showed no B_0 dependence, and multiple field data would generally fit to models of very slow exchange, with $p_A = p_B = 0.5$.

To quantify the effective $^{13}C-^{13}C$ coupling constants in the $^{13}CH_3$-pyruvate-derived WT* sample, a homonuclear carbon long-range coupling experiment was performed.[33] The results of the coupling experiment are given in Table 2. The small apparent coupling constants (<2 Hz) for many methyl carbons indicate that their effective relaxation rates will not be markedly affected by Hartmann−Hahn mixing during the CPMG intervals. Indeed, simulations have established that, for $^nJ_{CC} = 2.0$ Hz, contributions to $R_{ex} = R_{2,eff}(\nu_{CPMG} \rightarrow 0) - R_{2,eff}(\nu_{CPMG} \rightarrow \infty)$ that derive exclusively from this long-range coupling are less than 0.8 s^{-1}, while for coupling values of 0.5 Hz this contribution to R_{ex} drops to less than 0.1 s^{-1}. Thus, the small two-bond coupling between the fully labeled methyl groups in Leu and Val can safely be assumed not to interfere with echo formation during CPMG pulse trains (see Table 2).

In contrast, substantial $^3J_{C\delta C\alpha}$ couplings were measured for one of the two methyl groups in many of the Leu residues, indicating a significant three-bond $^{13}C\delta-^{13}C\alpha$ coupling in these cases, in addition to high levels of $^{13}C\alpha$ enrichment. In fact, the ^{13}C incorporation at the α positions of Leu residues is almost complete, due to a specific biosynthetic route where the $^{13}C\alpha$ label is derived from the acetyl-CoA methyl group, which in turn originates from the labeled pyruvate methyl group.[36,37] In these cases, there was little mobility about the χ_2 dihedral angle with $\chi_2 = 60°$ or 180° and the values of the coupling constants agree well with those predicted from dihedral angles obtained from crystal structures of T4 lysozyme.[40,41] For a number of Leu residues, Leu7, -32, -66, and -164, considerable rotomeric averaging was observed as established by averaged $^3J_{C\delta C\alpha}$ coupling values and low-order parameters obtained from ^{2}H spin relaxation data.[27] In cases where $^3J_{C\delta C\alpha} \sim 3-4$ Hz, contributions

Table 2. Effective Long-Range $^{13}C-^{13}C$ Coupling Constants Observed for $^{13}CH_3$-WT* T4 Lysozyme

residue type	coupling[a]	value (Hz)
Leu[b]	$^3J_{C\delta C\alpha}$	2.5−4.5
Leu[b]	$^3J_{C\delta C\alpha}$	0.7−1.8
Leu	$^2J_{C\delta C\delta}$	<0.5[c]
Val	$^2J_{C\gamma C\alpha}$	<0.5[c]
Val	$^2J_{C\gamma C\gamma}$	<0.5[c]
Ile	$^3J_{C\delta C\alpha}$	1.8−3.5[d,e]
Ile	$^2J_{C\gamma C\alpha}$	0.5−1.0
Ile	$^3J_{C\delta C\gamma}$	0.8−2.0
Ile	$^3J_{C\gamma C\delta}$	0.6−1.4
Met	$^3J_{C\epsilon C\beta}$	0.5−2.0

[a] The measured couplings have not been corrected for the isotope enrichment level and therefore are lower bounds. Couplings are extracted from a long-range quantitative *J* experiment that measured the ratio of diagonal to cross-peak intensities[33] (see Materials and Methods). Couplings denoted by $^nJ_{CkCl}$ were obtained by measuring the amount of magnetization transferred from *Ck* (diagonal) to *Cl* (cross-peak) and depend on the enrichment at *Cl*. For this reason $^nJ_{CkCl} \neq {}^nJ_{ClCk}$. For example, the C$\delta_1$ to Cγ_2 cross-peak is scaled by the enrichment at Cγ_2, and vice versa. The measured effective coupling is, therefore, not symmetric. [b] Leucine couplings have been separated according to those measured for methyl carbons that are trans (top line) and gauche (second line) to the Cα, determined on the basis of the crystal structures of L99A (pdb access code 1L90[40]) and WT* (pdb access code 1L63[41]). [c] No cross-peak could be detected. An upper limit was calculated from the noise level and a weak diagonal peak. For an intense diagonal peak, the detection limit was ~0.2 Hz. Lack of detection could also reflect spectral overlap, in which case it is not possible to exclude the possibility that couplings greater than 0.5 Hz are present. These couplings are, however, not expected to exceed 2 Hz. [d] Although some of these couplings are large (reflecting a high level of enrichment at Ile Cα) Ile δ_1 methyl groups are not considered in the experiments described. [e] Values for Ile9, Ile17, Ile27, Ile50, Ile58, Ile78, and Ile100 were all in excess of 3 Hz, indicating rather rigid trans configurations. This is in agreement with the X-ray structures mentioned under *b*, with the exception of Ile50, which is found in a g- configuration in the crystals. Smaller values of $^3J_{C\delta C\alpha}$ may be due to gauche configurations or increased conformational averaging. For example, the reduced ^{2}H order parameter ($S^2 = 0.45$) and small coupling constant ($^3J_{C\delta C\alpha} = 2.2$ Hz) for Ile3 are indicative of motion about χ_2. The rather high ^{2}H order parameter ($S^2 = 0.73$) but relatively small coupling constant ($^3J_{C\delta C\alpha} = 1.9$ Hz) for Ile150 may be interpreted as a rather rigid gauche configuration, although this bond is trans in crystals. This situation could alternatively be explained by slower (μs−ms time scale) partial averaging about χ_2, which does not affect quadrupolar relaxation.

(40) Eriksson, A. E.; Baase, W. A.; Matthews, B. W. *J. Mol. Biol.* **1993**, *229*, 747−769.
(41) Nicholson, H.; Anderson, D. E.; Dao-pin, S.; Matthews, B. W. *Biochemistry* **1991**, *30*, 9816−28.
(42) Markley, J. L.; Jorsley, W. J.; Klein, M. P. *J. Chem. Phys.* **1971**, *55*, 3604−3607.
(43) Patt, S. L. *J. Magn. Reson.* **1992**, *96*, 94−102.
(44) Boyd, J.; Soffe, N. *J. Magn. Reson.* **1989**, *85*, 406−413.
(45) Shaka, A. J.; Keeler, J.; Frenkiel, T.; Freeman, R. *J. Magn. Reson.* **1983**, *52*, 335−338.
(46) Marion, D.; Ikura, M.; Tschudin, R.; Bax, A. *J. Magn. Reson.* **1989**, *85*, 393−399.
(47) Neri, D.; Szyperski, T.; Otting, G.; Senn, H.; Wüthrich, K. *Biochemistry* **1989**, *28*, 7510−7516.
(48) Koradi, R.; Billeter, M.; Wüthrich, K. *J. Mol. Graphics* **1996**, *14*, 51−55.

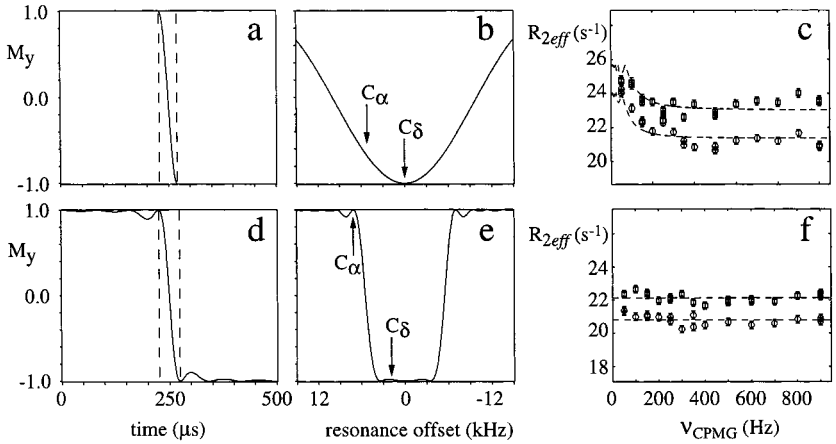

Figure 4. Comparison of square and band-selective REBURP 180° pulses for use in ^{13}C CPMG experiments. Simulations of the trajectories of *y*-magnetization during 40 μs rectangular (a) and 500 μs REBURP (d) refocusing pulses, with peak rf fields of 12.5 and 12.2 kHz, respectively. Note that the pulses deposit very similar amounts of power to the sample. Simulated excitation profiles for the hard (b) and REBURP (e) pulses. The pulses are applied at 21 (hard) and 8 ppm (REBURP, 600-MHz spectrometer frequency), with arrows indicating the resonance positions of the Cα and Cδ spins, with respect to the carbon carrier. Experimental dispersion profiles obtained for WT* Leu46δ_2, using rectangular (c) or REBURP (f) pulses at 600 (circles) and 800 MHz (squares).

to dispersion profiles from magnetization transfer can be considerable, as illustrated below (see Figure 4).

With this problem in mind we have replaced the rectangular nonselective refocusing pulses that we had been using during the CPMG trains with REBURP, methyl-selective pulses that refocus the $^3J_{C\delta C\alpha}$ couplings. Although REBURP pulses are longer than hard pulses, the majority of the rf is concentrated during a relatively small portion of the shaped pulse. It is therefore not surprising that the trajectories of transverse magnetization during hard and REBURP 180° pulses with similar peak rf fields (panels a and d of Figure 4) are nearly identical. The excitation profiles of hard and REBURP pulses, shown in panels b and e, are, however, very different. In practice, refocusing pulses in CPMG experiments were kept reasonably short (40 μs) to avoid off-resonance effects. Unfavorably, such short square pulses also excite Cα resonances (see Figure 4b) and lead to a pulse spacing-dependent modulation of $R_{2,\mathrm{eff}}$. This modulation can be eliminated by choosing the REBURP pulse width so that a null in the Cα region is obtained (for L99A, the Leu Cα resonances lie in a narrow region between 54.0 and 58.2 ppm). For example, at 600 (800) MHz, a 500 μs REBURP pulse was used, centered at 8 (20.2) ppm, illustrated in Figure 4e (600 MHz). This pulse refocuses the methyl region to greater than 98% while exciting Cα spins to less than 3%. Experimental methyl relaxation dispersion profiles obtained for Leu46δ_2 in WT* with hard and REBURP shaped refocusing pulses are shown in Figure 4c and f, respectively. The 4.5-Hz long-range coupling for this methyl resulted in artifactual relaxation profiles when hard pulses were used (panel c). Although each profile could be individually well fit with the fast-exchange equation, a poorer fit is generated when data obtained at two spectrometer fields are analyzed. However, when band-selective pulses are used, net evolution due to the scalar coupling is eliminated and the dispersion is flat (panel f).

Numerical simulations of the McConnell equations[34] were performed to establish that the use of long band-selective pulses does not interfere with extraction of accurate exchange parameters from fits of relaxation dispersion profiles in the present case. Using the same conditions as in the actual experiment, along with the fitted parameters for the exchange process in L99A ($k_{ex} \sim 1450\ s^{-1}$ and $p_B = 3.4\%$), constant-time relaxation

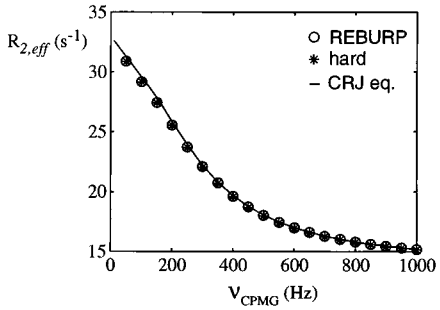

Figure 5. REBURP−CPMG dispersion profiles for a single spin undergoing two-site exchange. Exchange parameters, $\tau_{ex} = 0.69$ ms, $p_B = 3.4\%$, $\omega_A = 0$ ppm, $\omega_B = 1.1$ ppm (166 Hz for ^{13}C on a 600-MHz spectrometer), were used in the simulation. Circles indicate the calculated profile obtained by solving the homogeneous form of the McConnell equations,[34] including evolution during the REBURP pulses. The symbol * is used to show the profile calculated when the pulse width is zero, while the full line is the dispersion curve obtained using the approximate analytical expression of Carver and Richards[26] and Jen[30] (CRJ equation).

dispersion profiles were generated as described in Materials and Methods. An example of one such generated dispersion profile using 500 μs REBURP pulses is illustrated in Figure 5 (o) for $\delta\omega = 1.1$ ppm. Also indicated in this figure are dispersion profiles obtained assuming an infinitely short pulse (*), and it is clear that there are no contributions from exchange during the finite pulses in this example. As a point of interest, we have also included the predicted exchange profile obtained using the CRJ equation[26,30] (full line) based on the exchange parameters given above. Recall that the CRJ equation is approximate with better accuracy for faster exchange processes. As described in Materials and Methods, CRJ fits of the dispersion profiles generate exchange parameters that differ by no more than 2% from parameters extracted using the exact analytical expression for exchange. Not surprisingly, therefore, the CRJ-derived curve lies very close to the other profiles in the figure. Dispersion profiles have also been generated for $\delta\omega = 2$ ppm, $k_{ex} \leq 20\,000$ and $p_B \leq 10\%$ using both 500 μs REBURP and 40 μs rectangular refocusing pulses. In all cases for which $R_{ex} \leq 50\ s^{-1}$, we find that the average difference between $R_{2,\mathrm{eff}}(\nu_{CPMG})$ rates obtained using REBURP and rectangular pulses (50 Hz $\leq \nu_{CPMG} \leq 1$ kHz) and a given set of (ω_A,ω_B,k_{ex},p_B) values is

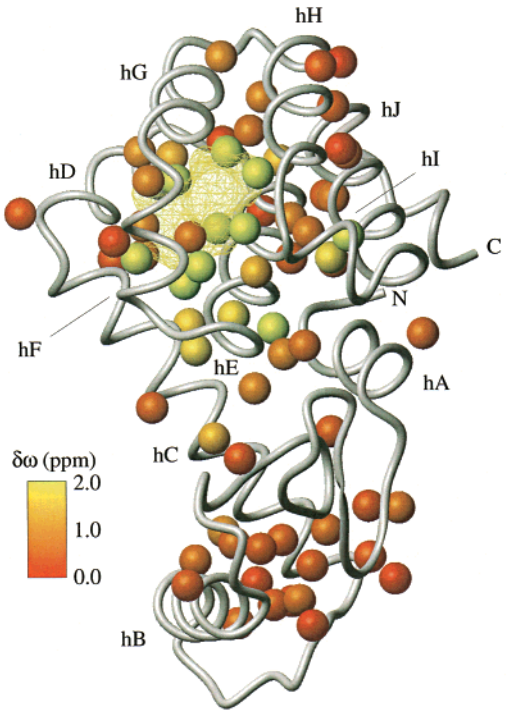

Figure 6. Three-dimensional representation of T4 lysozyme L99A. The N- and C-termini and all helices are labeled. Spheres designate methyl carbon atoms which are color-coded from red (no exchange) to yellow (exchange) according to the value of the per-residue chemical shift difference ($\delta\omega_{group}$) between exchanging sites obtained from the global fit of the dispersion data to a collective two-site exchange model.[29] The internal cavity is represented by a yellow wire frame cage. Figure prepared with MOLMOL.[48]

no greater than 0.8 s^{-1}. As described above, errors in rates on this order are also obtained from magnetization transfer due to nonvanishing long-range couplings as well as off-resonance effects. Notably, average differences between $R_{2,eff}(\nu_{CPMG})$ rates never exceed 2 s^{-1} even when the profiles have dispersions as large as 90 s^{-1}.

Access to Excited States and Ligand Exchange in L99A. As can be seen from Table 1, the exchange rates and populations extracted from the dispersion profiles are very similar for many of the probes. As a result, all of the methyl data were fit to a model in which the protein is exchanging between two conformations via a single, cooperative process. Only those residues with dispersion profiles satisfying the condition $R_{2,eff}(\nu_{CPMG} = 100\ Hz) - R_{2,eff}(\nu_{CPMG} = 900\ Hz) > 1\ s^{-1}$ at 800 MHz were included in the analysis. Notably, reduced χ^2 values increased by only 22% relative to values obtained from fits on an individual residue basis. The chemical shift differences between the ground state and the excited state, determined from the global fit, $\delta\omega_{group}$, were obtained for all methyl groups and are also reported in Table 1. Global values of $1/k_{ex} = 0.69$ ms and $p_B = 3.4\%$ are obtained; these values are within 2% of those calculated from a smaller number of reliable dispersion profiles measured with rectangular ^{13}C refocusing pulses.[29] Significantly, all large-amplitude dispersion profiles could be explained by the group fit.

The chemical shift difference for each individual methyl group derived from the group fit has been color coded onto the three-dimensional structure in Figure 6. Evidently, large perturbations in the local magnetic environment are present for nuclei that are close to the cavity. The spatial clustering of these nuclei and the fact that they have similar exchange times provides compelling evidence that these residues are involved in the same dynamic process. Moreover, the fact that the k_{ex} values determined are on the order of the rate of exchange of benzene from the cavity (800 ± 200 s^{-1} at 20 °C)[25] strongly suggests that the dynamic process described here is related to an opening event that is a prerequisite for ligand binding.

Conclusions

A buried cavity mutant of T4 lysozyme (L99A) was enriched with ^{13}C at 80 methyl sites by overexpression of the protein using $^{13}CH_3$-pyruvate as the sole carbon source. Although ^{13}C labeling was largely restricted to methyl positions in the protein, a detailed analysis of the long-range $^{13}C-^{13}C$ couplings involving labeled methyl groups indicated a high level of enrichment at the Cα positions of Leu residues. The 3−4 Hz $^3J_{C\delta C\alpha}$ coupling observed for some Leu methyls complicates the extraction of accurate exchange parameters for these groups when nonselective refocusing pulses are employed during the CPMG pulse trains in the experiment. The use of band-selective pulses has been shown to eliminate this problem. The transverse ^{13}C relaxation dispersion profiles obtained for side-chain methyl groups have allowed a detailed description of the internal dynamics of L99A on the millisecond time scale. It is anticipated that this methodology will find application to many protein systems.

Acknowledgment. We thank Dr. Ranjith Muhandiram for assistance with the long-range coupling experiment. F.A.A.M. was a postdoctoral fellow with support from the European Molecular Biology Organization (EMBO). The research was supported by grants from the Natural Sciences and Research Council of Canada (L.E.K.), AstraZeneca U.K. (L.E.K.), and the National Institutes of Health (Grant GM57766) (F.W.D.). L.E.K. is a foreign investigator of the Howard Hughes Medical Research Institute.

JA0119806